STAR Magnetic Fields and the Addition of the Endcap Electromagnetic Calorimeter

October 16, 2000

STAR Note 426

J. Sowinski

Indiana University Cyclotron Facility, 2401 Milo B. Sampson Ln., Bloomington IN 47408
sowinski@iucf.indiana.edu

Abstract

Installation of an Endcap Electromagnetic Calorimeter into the STAR magnet will require modifications and the addition of structures that have the potential to affect the internal magnetic field. Magnetic field calculations from a finite element analysis program are used to study a small modification to a feature in the poletip to mount the detector, the addition of magnetic steel PMT boxes to the outside of the west poletip and to set specifications on the stainless steel used in the structure of the EEMC. It is found that, in all cases, the effects on the field will be small compared to requirements on the field uniformity for tracking in the TPC.

1 Introduction

The purpose of this Star Note is to document the results of investigations into the effects on the STAR magnetic field that may arise from the addition of the Endcap Electromagnetic Calorimeter (EEMC). There are strict field uniformity requirements from the TPC. The magnet was mapped before TPC installation and will not be mapped again. Thus new installations should not change or distort the field substantially. Three specific effects have been considered. First: the method of hanging the upper half of the EEMC is to rework the plug in the lifting hole at the top of the west poletip to include a stainless steel cap from which the EEMC can hang. The effects of replacing some of the pin with stainless steel are evaluated. Second: Photomultiplier tube boxes will be placed directly on the west poletip's outer surface. The field is very high in this region requiring a lot of steel to shield the tubes. This has the potential to affect the internal fields and, since the boxes can not be placed in the region of the poletip lifting fixture, has the potential to add a ϕ dependence to the field. Third: The backplate and hub of the EEMC will be made of stainless steel. Certain grades of stainless steel, such as 316 and 304, are generally non-magnetic, even when cold worked or welded, but there is a wide range of chemical composition within these designations with varying propensities to become magnetic when worked.

Below I will first discuss the field uniformity requirements and then the methods of magnetic field calculation along with comparisons to measured fields. Next I describe the expected effects of the pin and PMT boxes and lastly set a specification on the permeability of the stainless steel for the EEMC structure.

2 Field uniformity requirements

The requirements on field uniformity are determined by allowable drift distortions in the TPC. This is described in the STAR Conceptual Design Report. For our purposes the concern is radial magnetic field components causing ϕ coordinate shifts, and to a lesser degree ϕ field components generating radial coordinate shifts, which result in errors in momentum determination. To produce the resolution needed, the integral of the fractional radial component must meet the following condition (Eq. 4C-6 in the STAR CDR)

$$\left| \int_z^{2.1m} \frac{B_r}{B_z} dz \right| \leq 0.7\text{mm}$$

where the integral is from the point of charge generation to the end of the TPC. With an average z component of 5000 G and the longest drift path of 2.1 m the average r component over the TPC would have to be <2 G. However, if the field is well mapped and software corrections can be performed, this requirement softens by about an order of magnitude. Such mapping has been done for the STAR magnet but will not be repeated. Thus in making our modifications for EEMC

Table 1: Coil currents used in calculations

Coil	Current (Amps)
Main	234,400
Space Trim	124,300
Poletip Trim	163,000

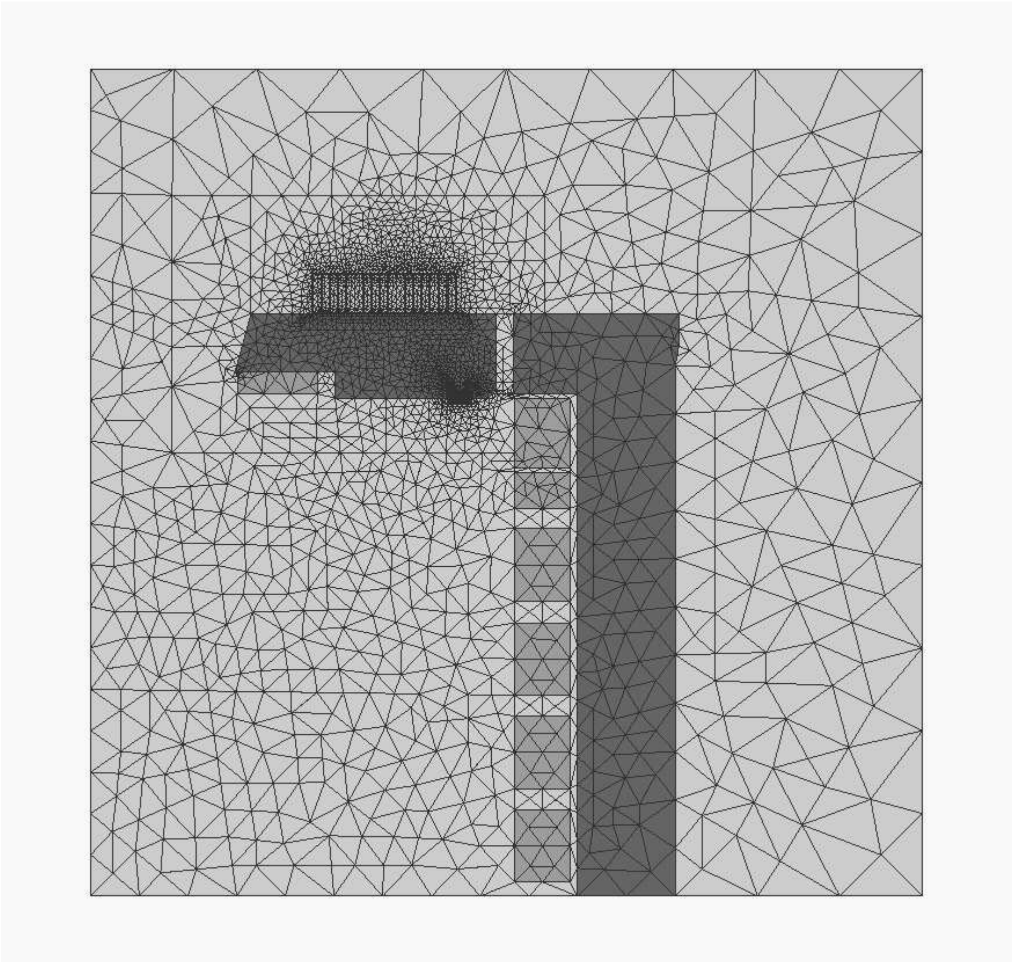

Figure 1: *An initial mesh for a quarter section of the magnet. In standard STAR coordinates (x,y,z) = (0,0,0) is located at the lower left of the figure. This sort of mesh was used in 2D calculations and uses many small elements near the plug in the poletip and the PMT boxes on the outside of the poletip.*

installation this integral should be perturbed by less than 0.7 mm. A similar integral should apply to ϕ components of the field, but is not made quantitative in the CDR. Howard Wieman (private comm.) quotes a limit of 0.2mm.

3 Method of calculation

The program MagNet from Infolytica was used for all calculations. This program allows both 2D and 3D calculations to be performed but most of the calculations were carried out as axisymmetric 2D calculations. Only the possible ϕ dependence from the addition of the PMT boxes utilized the 3D calculation capability of the program. The magnet geometry was drawn in a CAD program from STAR drawings and imported into MagNet. For 2D calculations the geometry was followed in detail. For the 3D calculations some simplifications were used to reduce the problem size.

The program allows for automatic meshing of the geometry but it was found necessary to subdivide line segments by hand to get appropriate meshing due to the small details investigated in such a large device. An example of an initial finite element mesh is shown in Fig. 1. Note that

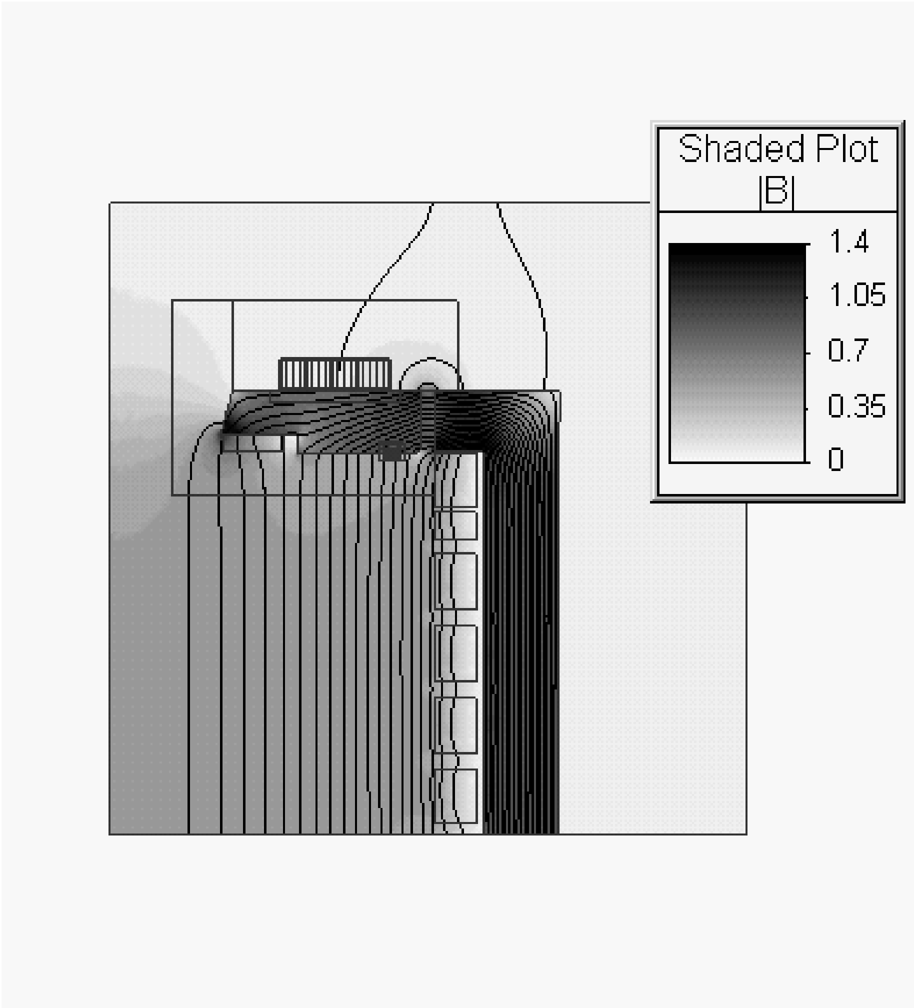

Figure 2: *Magnetic fields calculated for the STAR magnet with no EEMC modifications. The legend is in Teslas. The upper boundary is set to require normal fields on that surface, which seems to give better agreement with actual measurements of the magnet.*

geometry for the pin modification and PMT boxes is included.

In Fig. 2 the results of 2D calculations of the standard STAR magnet configuration are displayed. The currents used, listed in Table 1, are standard for full field. Magnetization curves contained in the MagNet program for 1010 cold rolled steel were used for the magnet components. The coils were set to aluminum and the rest to air. The convergence of the calculation can be judged by smoothness of the solution, stability with respect to remeshing and changing solution parameters such as polynomial order, and by checking field error plots generated by the program. The calculations presented here all appear to have converged and have errors less than the precision considered.

Shown in Fig. 3 are the calculations compared to measured field maps obtained from Steve Trentalange. Both radial and axial fields are plotted. Also shown are calculations where the outer boundary parallel to the poletip was set to normal boundary conditions rather than parallel (hereafter referred to as "modified boundary conditions"). This appears to give slightly better agreement with the measurements. It is unclear whether this is mocking up some effect of the

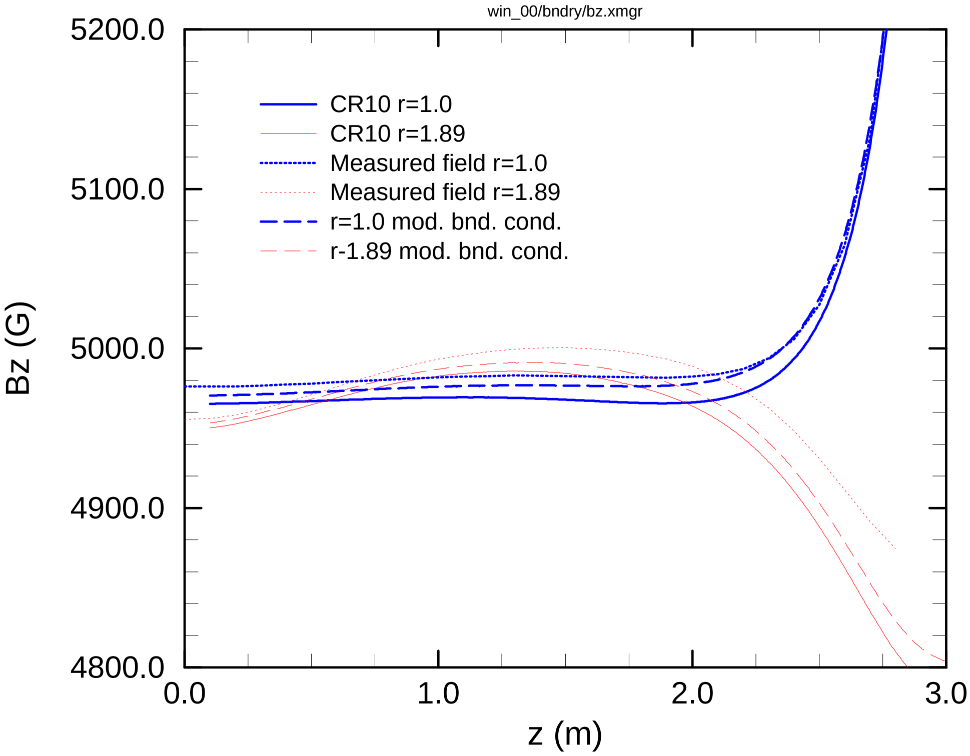

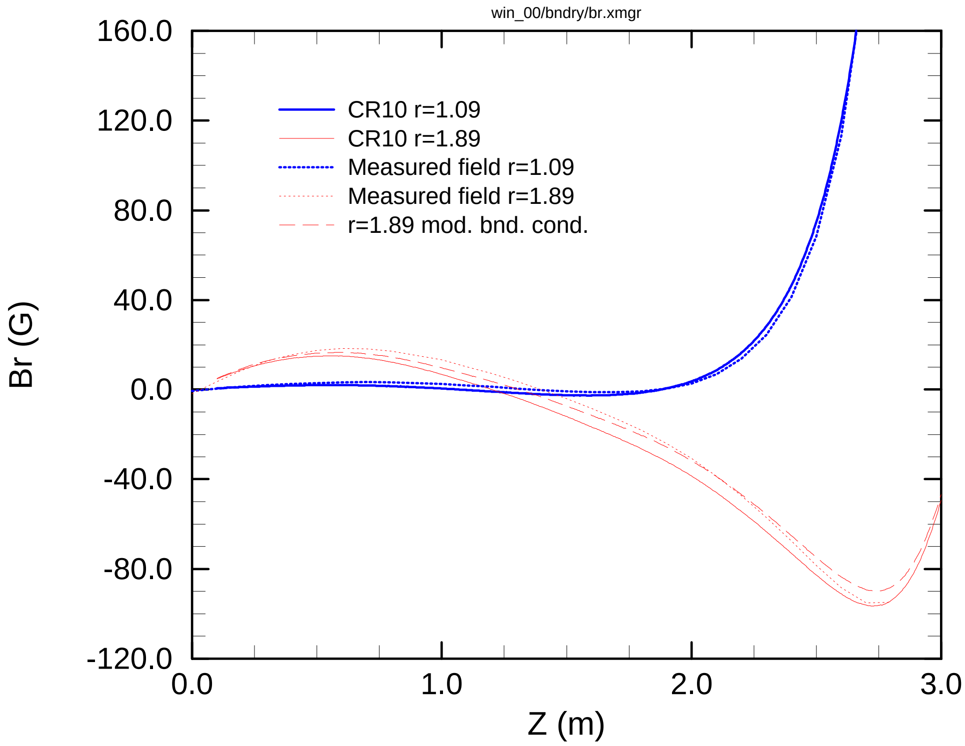

Figure 3: *The r and z components of the magnetic field for the standard STAR geometry. The calculations are compared to measured field maps. A second calculation with modified boundary conditions (as described in the text) is also shown and agrees with the measurements a bit better.*

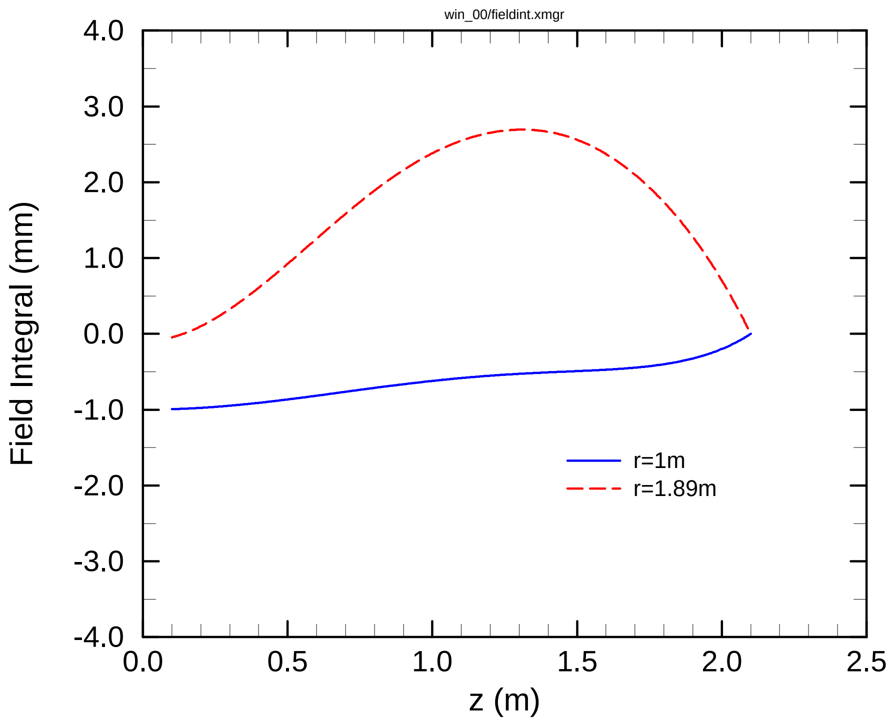

Figure 4: *The integral of fractional radial component vs. position of interaction in the TPC as expressed by the equation in Sect. 2. The integral is generated from the calculations in Fig. 3 using the modified boundary condition.*

poletip carriage and surrounding building structures or maybe the upper boundary was placed too close to the poletip in the calculation. In either case, the general features of the measured fields are well reproduced and quantitative agreement is at the Gauss level. The integrated radial field component is plotted against the point of charge generation in Fig. 4 for the calculation with the modified boundary condition. The integrated radial components are larger than the 0.7mm drift requirement stated in Sect. 2, particularly near the OD of the TPC, but still well within the correctable limit of 7mm.

In Fig. 5 the calculations are compared to measurements taken by Steve Trentalange on the outside surface of the poletip. Again the data are well reproduced considering their rapid variation and the fact that the measurements were done by hand rather than with a sophisticated mapping apparatus. Here I also find that the modified boundary condition on the upper surface matches the data somewhat better than the standard calculation with parallel boundary conditions. In all further calculations described in this report the modified boundary condition was used.

From the agreement with the measurements I conclude we have a good calculational platform to use for judging how modifications to the magnet might affect the field uniformity in STAR.

4 Modification of the Lifting Plug

Near the upper edge of the poletip there is a 5" diameter hole that was originally used to lift the poletip. This is presently filled with a plug made of magnet steel. Our intention is to modify this pin to protrude into the magnet volume by 1.25" to allow us to hang the upper half of the

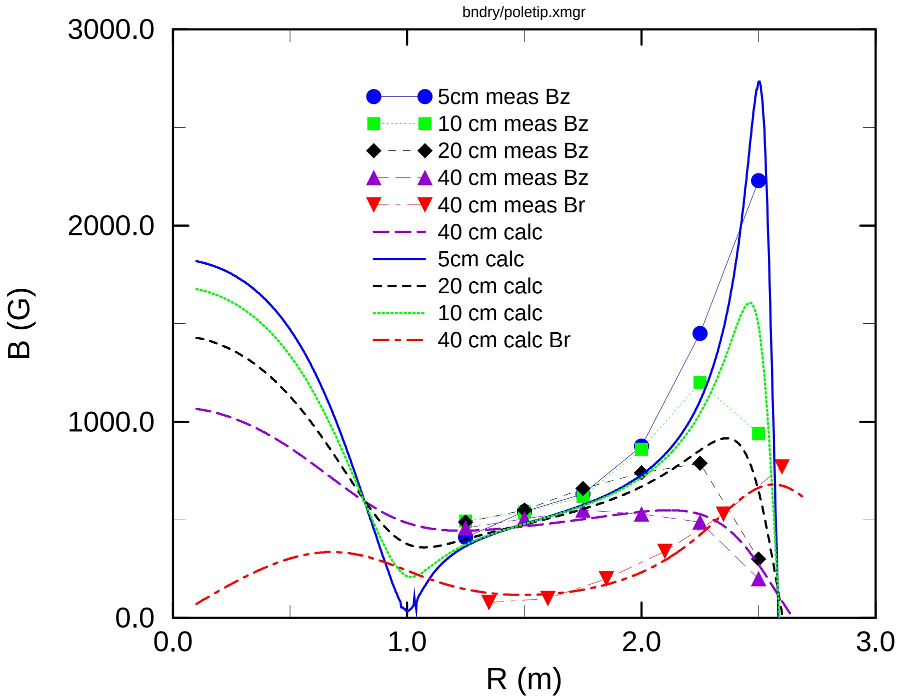

Figure 5: *The magnetic fields near the outer surface of the the poletip for the standard STAR geometry. The calculations are compared to field values measured by Steve Trentalange. For clarity, only calculations with modified boundary conditions are shown.*

EEMC from it. Such a protrusion can not be magnet steel for mechanical and magnetic reasons. The protrusion will be non magnetic stainless steel as shown in Fig. 6. Some of the existing pin near the surface will be removed to allow the stainless cap to bear on the walls of the hole in the poletip.

I have modeled this removal of magnet steel by putting air in the areas where stainless steel will be used. The calculation was done as a 2D calculation. Note that this is a gross overestimate since, in this axisymmetric model, it is the equivalent of having a circular groove on the face of the poletip, whereas the pin will only be a small feature in one location. The modified pin calculation is compared to the standard calculation in Fig. 7 along curves at the boundary of the TPC. Modifying the pin has virtually no effect on the field in the region of the TPC itself. This is because the steel nearby is not near saturation and the features of the hole are small compared to the distance to the region of high field uniformity requirements. Since the effect is already small in this overestimate, a 3D calculation was not pursued.

5 The Effect of PMT Boxes

As shown in Fig. 5 the fields on the back surface of the poletip are quite large. Considerable amounts of steel will have to be used to shield the photomultiplier tubes to be located there. Since there will be PMT boxes only on the west poletip a 2D calculation was run that included the full cross section of the STAR magnet, i.e. both east (with no PMT box) and west (with PMT boxes) halves, as shown in Fig. 8. The PMT boxes were modeled as solid magnet steel. Since this is a 2D calculation the boxes appear as a complete annulus. In reality only about 3/4 of the poletip surface

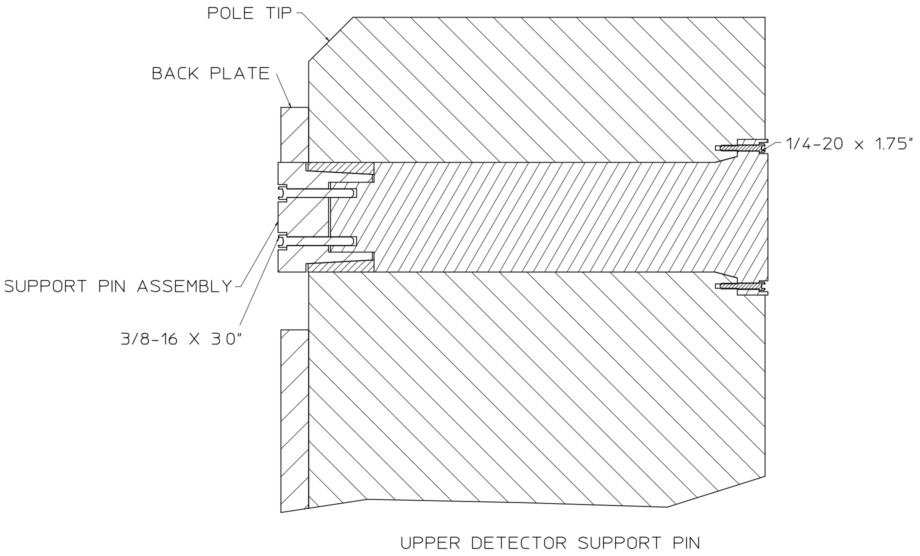

Figure 6: *Modifications to the magnet steel lifting pin plug. A stainless steel cap is added to provide a pin to hang the upper half of the EEMC. An expansion collar is used to get a tight fitting load bearing surface.*

will have PMT boxes on it because the poletip carriage attaches near the bottom. The boxes also will only cover about 1/2 of the available surface area. Thus the results of this calculation are an overestimate of the their effect by approximately a factor of 2.

Fig. 9 compares the fields inside the magnet with the installed steel PMT boxes to the standard calculation. It appears that the boxes increase the fields inside the magnet on the west side by 5-10 G, or about 1-2 parts per 1000. There are also a few Gauss changes in the radial fields. Fig. 10 shows the field integrals calculated in the same manner as Fig. 4. The integrals are typically altered by less than 0.7mm except at the outer diameter of the TPC near the west side of the center line where the difference is as large as 1mm. Given that the modeled PMT boxes overestimate the effects by about a factor of two or more, the changes in the integral for the installed boxes should not require corrections to the integrals derived from the measured field maps.

Nonuniformities or unwanted radial or azimuthal field components could arise from breaking of the magnet cylindrical symmetry by the PMT boxes. The boxes will not be continuous in ϕ as modeled so far but will be discreet boxes. More importantly, none can be placed in the region of the poletip carriage at the bottom of the poletip. This large gap could introduce ϕ components to the field.

To investigate the possible ϕ components introduced by the PMT boxes a 3D calculation was used. The geometry of the magnet and coils was simplified to minimize small features, allowing for larger mesh elements. For example, in this calculation the PMT box was solid without internal features, the mounting pin was not included, the poletip was squared off rather than tapered at the OD, and the coils were modified to eliminate small air gaps around them. The problem was also reduced in size by calculating only one quarter of the problem in ϕ. The PMT box was steel for 45° and air for 45°. With the boundary conditions imposed at the edge of the 90° slice modeled, I

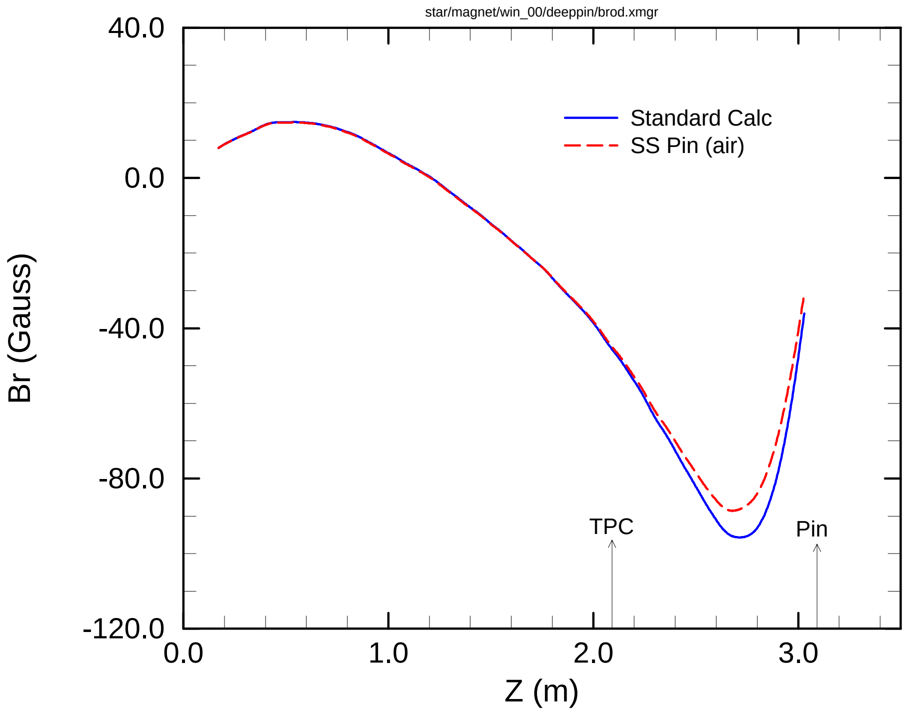

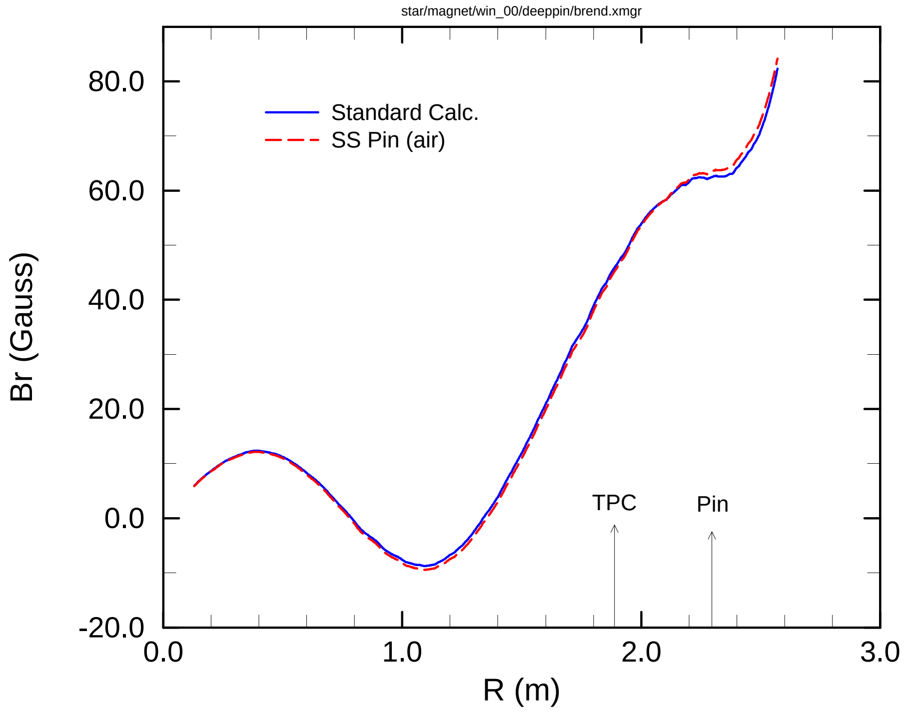

Figure 7: *Modifications of the magnetic field caused by adding a stainless steel cap to the lifting pin at the top of the poletip. The upper graph shows the radial field along the OD of the TPC. The lower graph shows the radial field along the end of the TPC. The limits of the TPC and the location of the pin are indicated.*

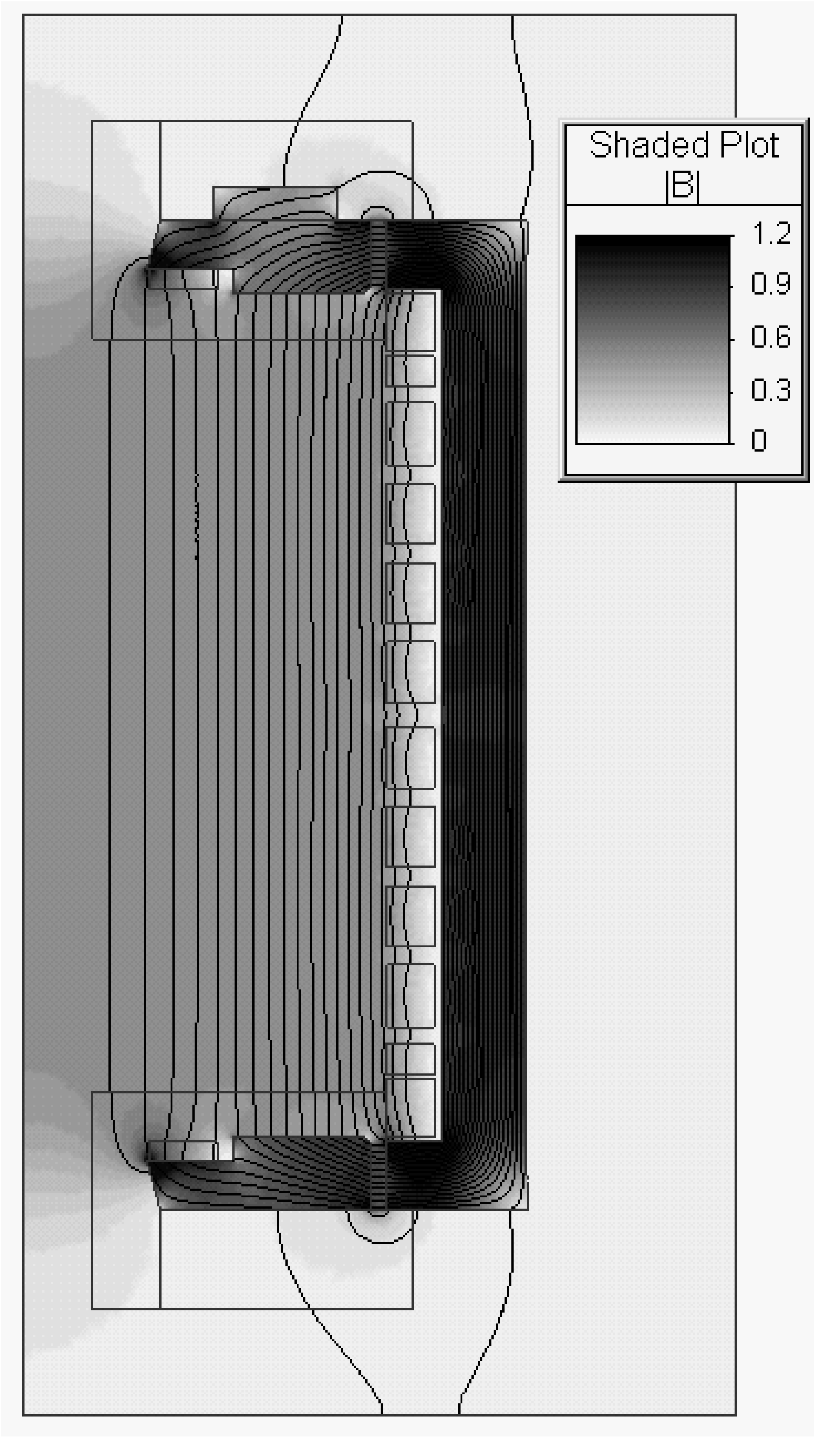

Figure 8: *A calculation with simulated PMT box on the west poletip. Here the full length of the magnet is modeled because the PMT box breaks the symmetry about Z=0.*

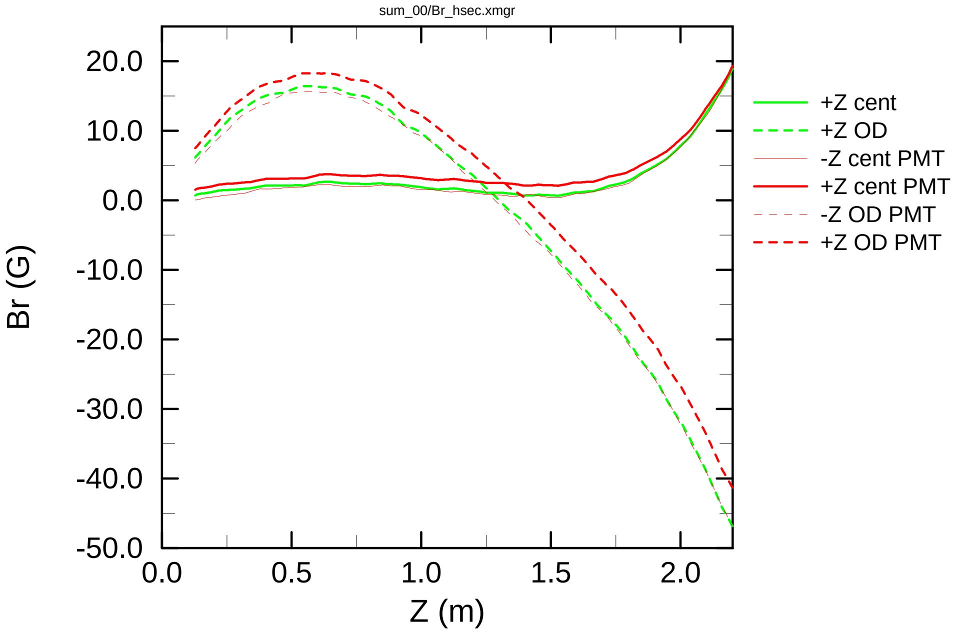

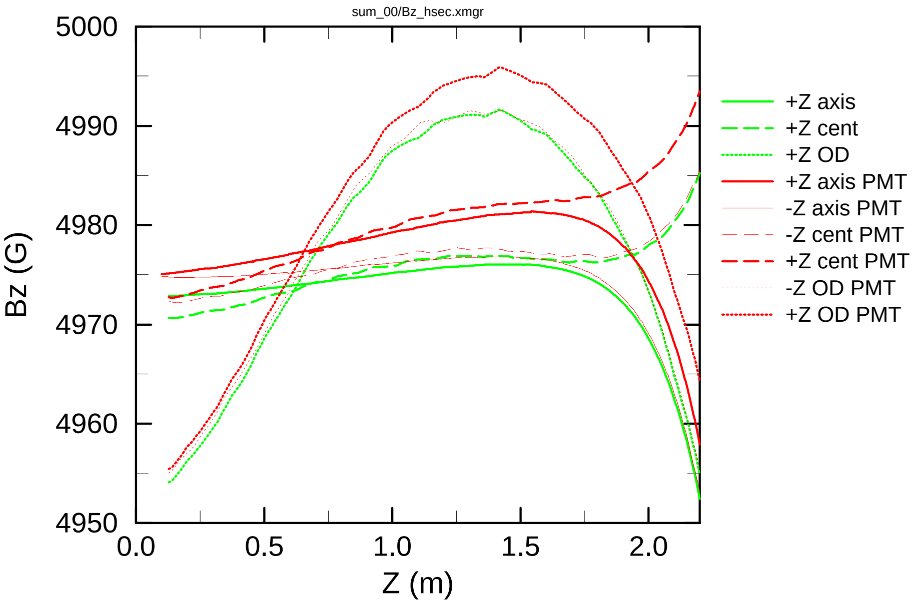

Figure 9: *Effect of adding the PMT boxes to the west poletip. Fields are shown on axis, at r=1 m (cent) and the OD of the TPC (r=1.89 m). The fields are symmetric about Z=0 without the PMT boxes. Fields with the PMT boxes for -Z have been overlaid on +Z for comparison.*

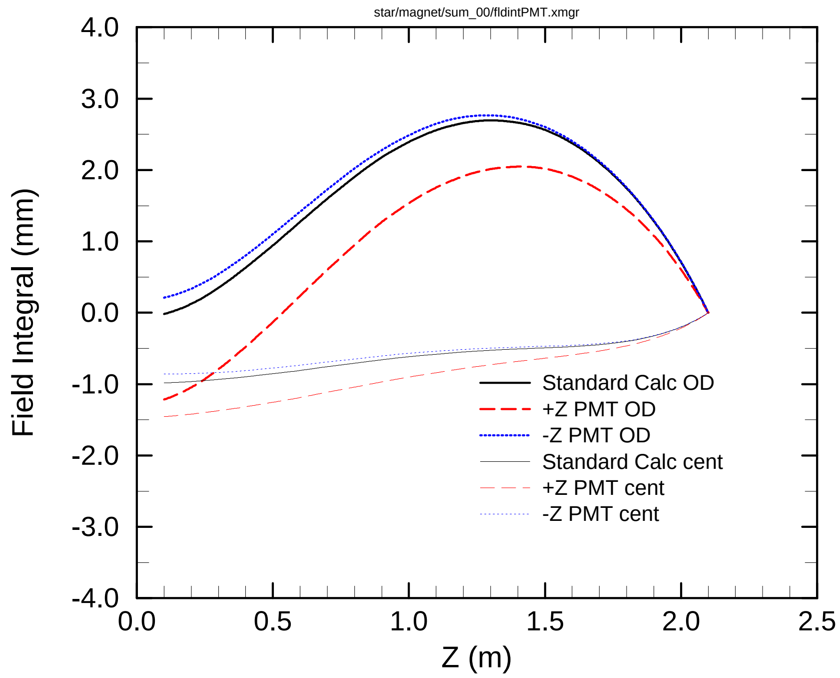

Figure 10: *Field integrals in the volume of the TPC with and without the PMT boxes on the west poletip. The standard calculation is the same as Fig. 4 except it is done with the full length magnet. The integral is performed at 2 radii, r=1.89 m (OD) and r=1.0 m (cent).*

am simulating alternating 90° regions of "boxes" and "no boxes".

The calculations show that the ϕ components of the field introduced in this way are small, typically less than 0.6 G, but are as large as 1 G near the OD of the TPC at some angles. The integral of the fractional ϕ component of the magnetic field is about 0.3mm in the worst case. This calculation is about a factor of 2 overestimate so no correction to the measured field maps should be necessary for this effect.

6 Calorimeter Structure

The main structural elements of the EEMC are a 1.25 in. thick backplate and a conical hub at η=2. These parts of the detector, as well as other components, will be made of stainless steel. Stainless steel alloys such as 304 and 316 are normally considered to be non-magnetic. Metals handbooks list the permeability of 304 (316) to range from 1.02 (1.003) when fully annealed to 7.0 (10.0) when severely cold worked. The propensity to become slightly magnetic when cold worked or welded is determined by the chemistry of the stainless steel, i.e., the amount of nickel-like (Mn,N,C) and chromium-like (Cr,Mo,Si) elements it contains. Even within the general classes of 304 and 316 stainless steel the concentrations of these metals can vary by 2-3%. At lower Ni-like and higher Cr-like concentrations δ-ferrite centers can form under cold working or welding. These centers are

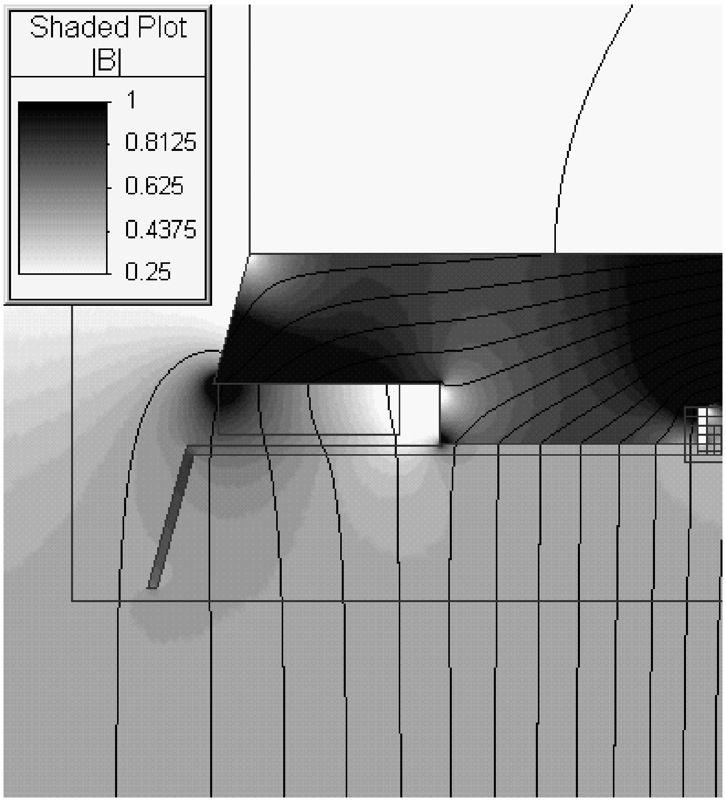

Figure 11: *A calculation of the magnetic fields with the stainless steel structure of the EEMC installed. The values are in Tesla. The permeability of the steel is set to be constant at 1.5. This is an overestimate of the effect because the stainless steel will most likely saturate at much lower fields than present at their location in the STAR magnet.*

magnetic and account for the increased magnetic properties. With annealing they are converted to non-magnetic austenite (see CERN Accelerator School Proceedings, CERN 94-01, V. II). If the concentrations of these elements are known for a particular sample of stainless steel, the amount of δ-ferrite that can be formed is determined from a graph called a Schaeffler diagram.

The range of Ni- and Cr-like concentrations that fall within the broad categories of 304 and 316 stainless steels include regions where there is no possibility of δ-ferrite formation. They also include regions where there could be as much as 20% δ-ferrite formation. This detailed study was prompted by information from the G0 experiment where they found that most manufacturers in the US tend to produce stainless steels in the ferrite forming ranges of the concentrations. (The problem is more severe for G0 due to their cryogenic application.) There is a range available and we can control possible problems by selecting materials for low δ-ferrite formation. For example, 316L stainless steel sheet ordered for Pb radiator lamination prototyping should have %5 or less δ-ferrite formation. This material was tested with a Severn gauge to have $\mu < 1.01$. I also tested

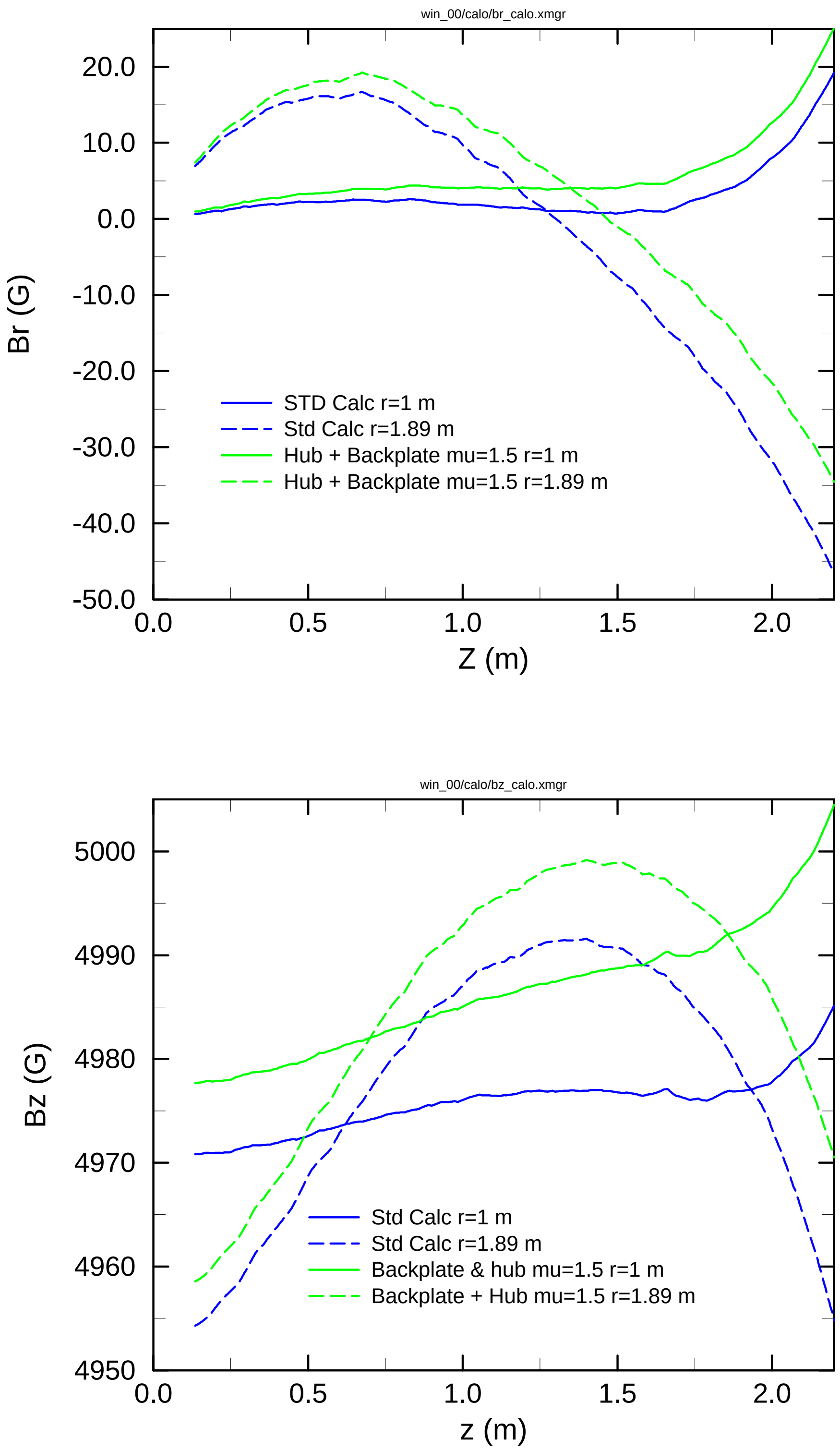

Figure 12: *Magnetic fields with a slightly magnetic EEMC structure installed in the STAR magnet. The permeability is set to be constant at 1.5. This overestimates the effect because the stainless steel is likely to saturate at the fields present in the region. Nevertheless we will set a limit of 1.2-1.3 on the permeability of materials to be used in the endcap and expect that values less than 1.1 will be achieved.*

seven samples of 304 and 316 sheet, bar and round stock of unknown chemistry taken from the IUCF machine shop. Four samples tested <1.01, the other three had edges and surfaces at 1.02 or greater but all less than 1.5. The elevated permeabilities seemed to be associated with ground or otherwise worked surfaces.

The design of the backplate and hub for the EEMC has evolved to a state where there is no welding done on the parts. The backplate is simply machined. The hub is cold worked from a plate into an annular piece but the deformation is only about 2%. The parts will be stress relieved via annealing but I believe this process is different than would be followed to magnetically anneal for the removal of the δ-ferrite components. In any case, I expect that, with the minimum cold working involved, there will be little increase in the permeability of the stainless steels used. We will ask the manufacturer to provide us with the chemistry of available materials and choose those that minimize δ-ferrite formation. We will also ask them to work a sample and anneal it similar to the process that will be followed for the hub and then test the sample with a Severn gauge before manufacturing the backplate and hub. Prototype small parts will also be checked before production.

In order to determine criteria for the allowable permeability in the hub and backplate I carried out magnetic field calculations using the same methods as above. These were 2D calculations in quarter section as shown in Fig. 11. In the results shown the permeability of the stainless steel was set to be constant at 1.5. This is an overestimate because the stainless steel will saturate at a fairly low field related to the δ-ferrite content. The results of the calculation are shown in Fig. 12. Here we see that the changes in the field are similar in magnitude to those caused by the addition of PMT boxes to the outside of the poletip. Setting a limit of 1.2-1.3 on the permeability of the EEMC structure as measured with a Severn gauge will be sufficient to prevent the need to correct the previously measured field maps. It is expected that permeabilities below 1.1 will be achieved.

7 Conclusion

The effects of adding the EEMC on the magnetic fields of the STAR detector have been explored, particularly as regards the field maps within the volume of the TPC. The reworking of a pin near the top of the poletip for mounting the upper half of the EEMC appears to be of no consequence. The detector structure should have little effect if the materials are controlled. The studies help establish criteria on the allowed permeability of the stainless steel used in the EEMC and there is every reason to expect suitable materials can be found. The addition of steel boxes to shield the PMTs for the calorimeter generate calculated field effects close to being large enough to require corrections only near the OD of the TPC. We expect the actual effects to be about a factor of 2 smaller and thus not large enough to require corrections even at the TPC outer diameter. Final checks using installed NMR probes and tracking cosmic rays can be performed after installation and before beam. In conclusion, it appears that the EEMC should not present any problems with the field maps as regards TPC tracking, which is the most stringent constraint on knowledge of the magnetic fields.